Surface & Coatings Technology 205 (2011) 5073–5076

Contents lists available at ScienceDirect

Surface & Coatings Technology

journal homepage: www.elsevier.com/locate/surfcoat

Negative thermal expansion ZrW_2O_8 thin films prepared by pulsed laser deposition

Hongfei Liu [a,*], Zhiping Zhang [c], Wei Zhang [b], Xiaobin Chen [b], Xiaonong Cheng [c]

[a] Testing center of Yang zhou University, Yang zhou, 225009, PR China
[b] School of Physics Science and Technology, Yang zhou University, Yang zhou, 225009, PR China
[c] School of Materials Science and Engineering, Jiang su University, Zhen jiang 212013, PR China

ARTICLE INFO

Article history:
Received 29 March 2011
Accepted in revised form 13 May 2011
Available online 23 May 2011

Keywords:
Negative thermal expansion
Zirconium tungstate
Thin film
Pulsed laser deposition

ABSTRACT

Negative thermal expansion ZrW_2O_8 thin films has been grown on quartz substrates by pulsed laser deposition (PLD) method followed by annealing at various temperatures. The influences of annealing temperature on the morphology and phase composition of the ZrW_2O_8 thin films were investigated. The X-ray diffraction (XRD) and X-ray photoelectron spectroscope (XPS) analyses revealed that the as-deposited ZrW_2O_8 thin film showed an amorphous phase, the stoichiometry of the as-deposited thin film was close to that of the ZrW_2O_8 ceramic target, the crystallized cubic ZrW_2O_8 thin films were prepared after annealing at 1200 °C. The scanning electron microscope (SEM) confirmed that the ZrW_2O_8 thin film deposited on the substrate heated at 650 °C was smooth and compact, the crystallized cubic ZrW_2O_8 thin film was a polycrystalline film and its grain size grew to be larger. The high temperature X-ray diffraction analyses showed that all the peaks ascribe to the ZrW_2O_8 thin film shifted to higher angle with the increasing temperatures, which demonstrated that the cubic ZrW_2O_8 thin film exhibited negative thermal expansion and its thermal expansion coefficient was calculated to be $-11.378\times10^{-6}K^{-1}$ from 20 °C to 600 °C.

1. Introduction

It is well known that the vast majority of materials expand on heating. Nevertheless, in recent years families of materials with a negative thermal expansion (NTE) have been discovered. The material ZrW_2O_8 is one of the best known which has stimulated considerable interest, because it has an exceptionally large($-8.7\times10^{-6}K^{-1}$) and isotropic negative thermal expansion over its entire stability temperature range from −273 °C to 770 °C [1–4]. This property leads itself as fillers to applications requiring dimensional thermal stability, which includes a wide variety of areas such as electronics [5,6], optics [7,8], sensors and actuators [9] materials. Early studies mainly focus on the preparation and characterization of ZrW_2O_8 powders and ceramics [10,11], and then the ZrW_2O_8 as a filler material is used to fabricate the controllable thermal expansion composites, such as ZrO_2/ZrW_2O_8 [12,13] and Cu/ZrW_2O_8[14–16]. But the published research literatures on ZrW_2O_8 thin films are still very limited. The properties of ZrW_2O_8 thin films may differ greatly from those of ceramic and powders due to the dimensional effect, and the negative thermal expansion thin films also have some irreplaceable use value, as we know, the surface functional coating layer or thin film is important to functional devices, and a mismatch in thermal expansion coefficient between the layered films and base materials can cause problems with changes in temperatures, such as mechanical destruction and positional deviation. The negative thermal expansion thin film may be useful for solving this problem, further research on ZrW_2O_8 thin film is thus very necessary.

So far, several preparation techniques have been described in attempts to synthesize ZrW_2O_8 thin films. For example, Sutton et al. [9] reported the ZrW_2O_8 thin films deposited by electron-beam evaporation and reactive cosputtering. However, the stoichiometry of the resulting thin film, ZrW_xO_y ($x\neq2$, $y\neq8$), differed from the ZrW_2O_8. Noailles et al. [17] prepared a ZrW_2O_8 thin film by depositing 0.5 mol/L ZrW_2O_8 sol onto silicon wafer and calcining at 1150 °C. In our earlier work, we also reported that the preparation of the ZrW_2O_8 thin films by radio frequency magnetron sputtering using the ZrO_2 and WO_3 composite ceramic target, but Xiao et al. [18] failed to obtain pure ZrW_2O_8 thin films due to the priority sputtering and volatilization of WO_3 at high temperature.

As is well known, the properties of the thin films are sensitive to their stoichiometry, microstructure and crystallinity which depend on the sputtering method and post-deposition processing conditions. Hence, these are also crucial to achieve high quality ZrW_2O_8 thin films. Pulsed laser deposition (PLD) is a versatile fabrication technique that enables to preserve the stoichiometry of the target while producing high-quality thin films. In this work, the NTE cubic ZrW_2O_8 thin films were synthesized by PLD method. The effects of annealing temperature on microstructure and growth morphologies of the thin film were investigated. A reproducible route of synthesizing both pure phase and negative thermal expansion thin films has been obtained.

* Corresponding author. Tel.:+86 514 87979022; fax: +86 514 87979244.
E-mail address: liuhf@yzu.edu.cn (H. Liu).

0257-8972/$ – see front matter © 2011 Elsevier B.V. All rights reserved.
doi:10.1016/j.surfcoat.2011.05.010

2. Experimental procedure

ZrW_2O_8 ceramic target was prepared by solid state reaction method, the WO_3 and ZrO_2 powders (99.95% purity) were milled for 48 h to form a uniform mixture of the stoichiometric ratio of 2:1. Then the powders were uni-axially, cold pressed into Φ23 mm × 4 mm target, calcined at 1200 °C for 4 h and quenched in de-ionized water to obtain the ZrW_2O_8 ceramic target.

The thin films were grown on quartz substrates (10 mm × 10 mm × 1 mm) by PLD method using a KrF excimer pulsed laser with a wavelength of 248 nm. Before deposition, the substrates were dipped in acetone to remove the surface contamination, rinsed with a large amount of de-ionized water, dried in a flux of N_2, and placed into the vacuum chamber with a base pressure of 2×10^{-3} Pa. The distance between target and substrate was 3.5 cm. The laser flux approximately was 356 mJ/cm^2 and repetition rate was 5 Hz. During deposition, the oxygen pressure was fixed at 10 Pa and the deposition time was 60 min. The thin films were deposited at 650 °C. After deposition, the as-deposited films were post-annealed at 740 °C, 800 °C, 900 °C, 1000 °C, 1100 °C, 1200 °C for better crystallization.

Structural characterization was carried out using XRD Rigaku D/max 2500 (CuKα radiation) analysis. The power of the XRD was fixed at 40 kV and 200 mA, the scanning speed of 2θ angle was 5°/min and the XRD diffraction angle (2θ) was measured from 10° to 60°, and the high temperature X-ray diffraction measurement was carried out using XRD Rigaku D/max 2500 (CuKα radiation) analysis, which were used to collect the resulting cubic ZrW_2O_8 thin films XRD date at different temperature room temperature, 100 °C, 200 °C, 300 °C, 400 °C, 500 °C and 600 °C, respectively. Surface morphologies of the as-deposited ZrW_2O_8 thin films and annealed thin films were studied using the Hitachi S-4800IIfield emission scanning electron microscope (FESEM). The composition of the as-deposited ZrW_2O_8 thin film was analyzed by Thermo ESCALAB 250 X-ray photoelectron spectroscopy (XPS) using focused monochromatic Al Kα radiation with energy of 1486.6 eV. In all cases surface charging effects were compensated by referencing the binding energy to the C 1s line set at 284.6 eV. The thicknesses of the thin films were measured by ET-350 surface profilometer.

3. Results and discussion

The stoichiometric ratio of thin film deposited by PLD method is always the same as the one of the target. So the purity of target as a raw material is vital to the quality of the thin film. Fig. 1 shows XRD patterns of the ZrW_2O_8 target synthesized by solid state reaction method. All the diffraction peaks are identified as the cubic unit cell of α-ZrW_2O_8 (JCPDS #50-1868) which indicates the resulting ZrW_2O_8 target is pure, and the indices of crystallographic plane of the resulting ZrW_2O_8 target are shown in Fig. 1.

All the thicknesses of the thin films deposited by PLD method in this study were approximately 400 nm. As shown in Fig. 2(a), the XPS analysis reveals that the atomic ratio of the element Zr, W and O of the as-deposited thin film is about 1.00:2.08:7.93, which is close to the one of the ZrW_2O_8 target. There is no impurity element, it is mainly because the ZrW_2O_8 ceramic target is pure and the laser is a clean energy source. The Element C comes from the oil pump. The carbon peaks (observed at 284.6 eV) can be used to calibrate the resulting spectra to account for any surface charging effects.

The XRD patterns of the ZrW_2O_8 thin films deposited at a substrate temperature of 650 °C and post-deposition annealed at various temperatures are shown in Fig. 3. The as-deposited ZrW_2O_8 thin film shows an amorphous phase. When the particles impinge on the substrate at 650 °C, maybe the energy is not adequate for these particles to form crystallized ZrW_2O_8 thin film. The post-deposition annealing is needed to change the amorphous structure and realize crystallization, so post-deposition annealing at different temperatures

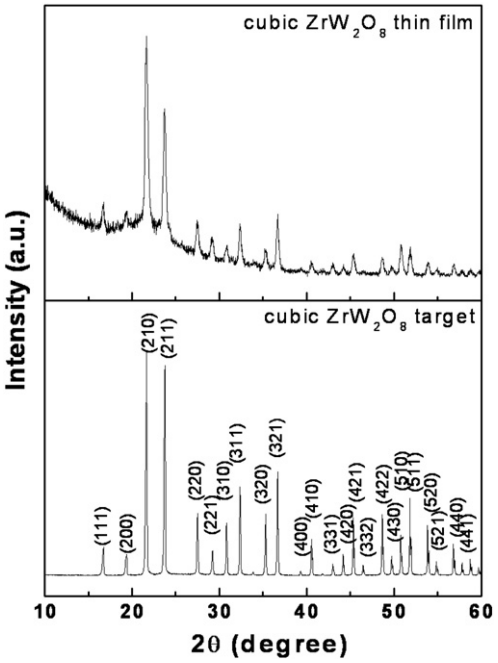

Fig. 1. XRD patterns of the cubic ZrW_2O_8 target and thin film annealed at 1200 °C.

was studied. When the amorphous thin films were annealed at 740 °C, 800 °C for 3 min in air, respectively, the peaks present in the XRD pattern of the thin film are assigned to the WO_3, and annealed at 900 °C, 1000 °C for 3 min in air, respectively, the peaks of tetragonal ZrO_2 and WO_3 present in the XRD patterns of the thin films. With the increase of annealing temperatures, the dominant XRD peaks became sharper and stronger due to the further enhancement in crystallization. However, when annealed at 1100 °C for 1 min in air, only the peaks of tetragonal and monoclinic ZrO_2 present in the XRD pattern and the XRD peaks of WO_3 disappeared due to the volatilization of WO_3 at high temperature. In order to avoid the volatilization of WO_3 and obtain the crystallized ZrW_2O_8 thin film, an improved annealing process was carried out by placing the as-deposited ZrW_2O_8 thin film in a sealed cell and then annealing at 1200 °C for 3 min. After quenching in de-ionized water, the cubic ZrW_2O_8 thin films of high purity were obtained for the first time, and the XRD pattern of the resulting cubic ZrW_2O_8 thin film is shown in Fig. 3. Compared with the one of the ZrW_2O_8 target, it obviously can be found that there is no impurity peaks in the XRD spectrum of the cubic ZrW_2O_8 thin film. The XPS analysis also reveals that the atomic ratio of the element Zr,

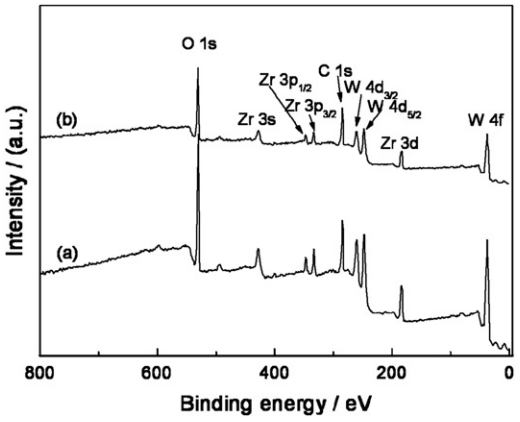

Fig. 2. X-ray photoelectron spectroscopy (XPS) spectra of the ZrW_2O_8 thin films, (a) as-deposited, (b) annealed at 1200 °C for 3 min.

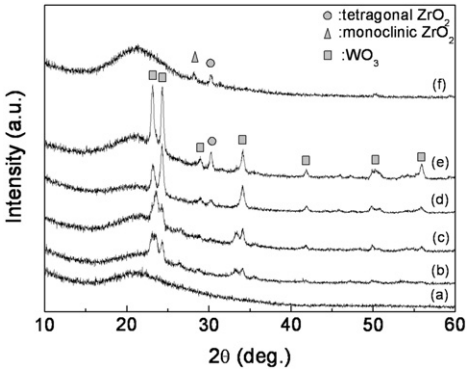

Fig. 3. XRD patterns of ZrW_2O_8 thin film annealed at different temperature (a) as-deposited, (b) annealed at 740 °C for 3 min, (c) annealed at 800 °C for 3 min, (d) annealed at 900 °C for 3 min, (e) annealed at 1000 °C for 3 min, (f) annealed at 1100 °C for 1 min.

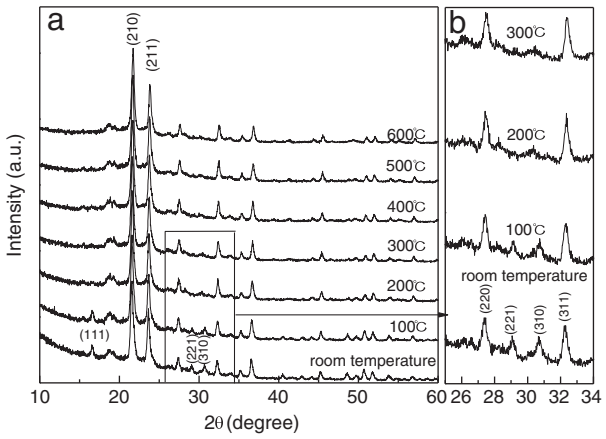

Fig. 5. High temperature XRD patterns of the cubic ZrW_2O_8 thin film at various temperatures.

W and O of the thin film annealed at 1200 °C is about 1.00:1.95:7.92 (see Fig. 1(b)), both the analysis of the XRD and XPS can confirm that the resulting sample is pure cubic ZrW_2O_8 thin film.

The surface morphologies of the ZrW_2O_8 thin films are inspected by FESEM. Fig. 4 shows the FESEM micrograph of the as-deposited ZrW_2O_8 thin film and annealed at 1200 °C, respectively. In Fig. 4(a), it can be seen that the surface micrograph of amorphous ZrW_2O_8 thin film deposited at a substrate temperature of 650 °C is smooth and compact, the surface of the film with characteristic absence of significant grain growth, which indicates the amorphous state of the thin film. The SEM micrograph of the cubic ZrW_2O_8 thin film annealed at 1200 °C for 3 min is shown in Fig. 4(b), where one can see that the crystallized ZrW_2O_8 thin film is a polycrystalline film, the grains on surface show a trend of merging to form bigger grains and there are lots of Y-grain-boundaries. But there are some cracks in the crystallized ZrW_2O_8 thin film. On one hand, this might be caused by the mismatch in thermal expansion coefficient between the thin film and the substrate. On the other hand, the quenching generates lots of stress. Both the reasons can lead to the crack deficiency.

To investigate the negative thermal expansion behaviors, the XRD patterns of the resulting cubic ZrW_2O_8 thin films were collected at various testing temperatures, which were displayed in Fig. 5. In Fig. 5(a), all the XRD peaks of the cubic ZrW_2O_8 thin film slightly shift to higher 2θ with the increase of the testing temperatures, which can be obviously found in Fig. 6. Fig. 6 exhibits the 210 peaks and 211 peaks of cubic ZrW_2O_8 thin film at various testing temperatures. Due to the cubic structure of the ZrW_2O_8 thin film, when the diffraction angle increases, value of d decreases in contrast, which lead to the decreasing of the lattice constants and contracting of the cell volume of ZrW_2O_8 thin film by increasing temperatures. This indicates that the resulting cubic ZrW_2O_8 thin film shows negative thermal expansion property, attributed to the rigid unit mode of its framework structure and the liberation of the WO_4 unit with the unshared vertex [19–21]. The lattice constants of the cubic ZrW_2O_8 thin films at various temperatures were calculated by the cell parameter calculation method using a powder X software [10,22]. Fig. 7 depicts the lattice constants of the cubic ZrW_2O_8 thin film depended on the temperatures, it can be obviously seen that the lattice constants decrease with the increasing temperatures, which also indicates that negative thermal expansion nature of the obtained ZrW_2O_8 thin film, and the average linear thermal expansion coefficient of the cubic ZrW_2O_8 thin film is calculated to be $-11.378\times10^{-6}\,K^{-1}$ in the temperature range from 20 °C to 600 °C using the linear regression technique, which agree with the negative thermal expansion coefficient of the ZrW_xO_y thin film ($14\pm4\times10^{-6}\,K^{-1}$) reported by M.S. Sutton [8], We can find that the average linear thermal expansion coefficient of the cubic ZrW_2O_8 thin film is more negative than that for the bulk ZrW_2O_8 reported elsewhere [1]. It is speculated that there are lots of reasons can lead to this phenomena, such as the difference on the preparation method, density, microstructure between the ZrW_2O_8 thin film and bulk. Furthermore, the annealing process of the thin film generates a large number of stresses due to the difference of the thermal expansion coefficient between the ZrW_2O_8 thin film and the substrate. All of these factors may have some affects on the measurement of the ZrW_2O_8 thin film. Further work is in the progress to investigate the formation mechanism in detail.

In Fig. 5(a), several XRD peaks of the cubic ZrW_2O_8 thin film such as the (111), (221) and (310) peaks that exist at room temperature. With the increase of testing temperatures, these XRD peaks disappeared at high temperature above 200 °C, and this phenomenon can be obviously seen in Fig. 5(b). This indicates that a structural phase transition from an acentric phase to a centric phase takes place in this temperature range from 100 °C to 200 °C. The low-temperature phase ($P2_13$) transits to the high temperature phase ($Pa\bar{3}$). ZrW_2O_8

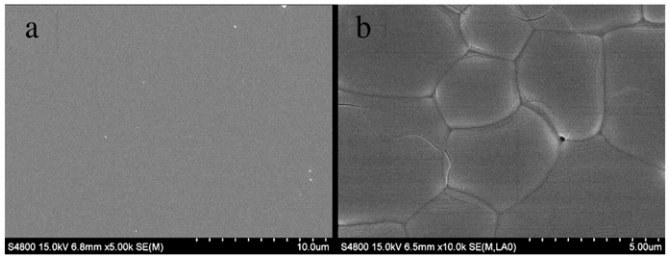

Fig. 4. FESEM images of the ZrW_2O_8 thin films for (a) as-deposited and (b) post-deposition annealed at 1200 °C.

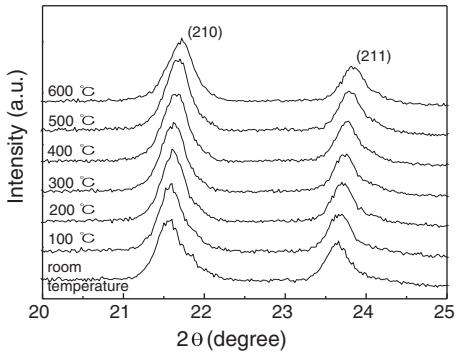

Fig. 6. 210 peak and 211 peak of cubic ZrW_2O_8 thin film at various temperatures.

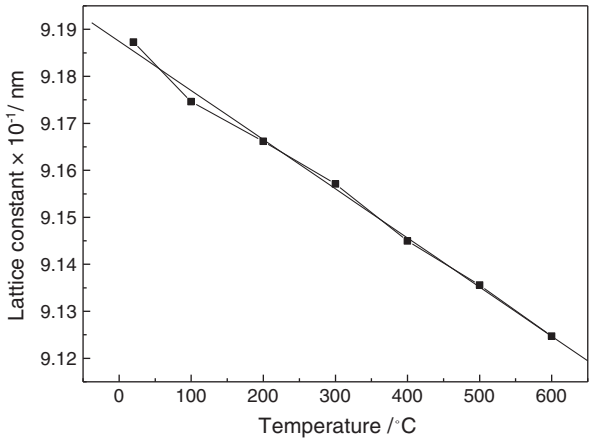

Fig. 7. The lattice constant depended on the temperatures for cubic ZrW_2O_8 thin film.

undergo an α to β structure phase transition between 100 °C and 200 °C, which is considered to be order–disorder type [2,9,10].

4. Conclusion

In summary, cubic ZrW_2O_8 thin films were successfully prepared by the PLD method using ZrW_2O_8 ceramic target. The ZrW_2O_8 thin film deposited at a substrate temperature of 650 °C was amorphous, and its surface micrograph was smooth and compact. The crystallization of the ZrW_2O_8 thin films was found to be dependent on the annealing temperature and process. The crystallized cubic ZrW_2O_8 thin film can be obtained after annealing at 1200 °C for 3 min in a sealed cell and quenched in the de-ionized water. There are lots of Y-grain-boundaries existed in the polycrystalline ZrW_2O_8 thin film. The obtained cubic ZrW_2O_8 thin film showed strong negative thermal expansion, its average linear thermal expansion coefficient was calculated to be $-11.378\times10^{-6}\,K^{-1}$ from 20 °C to 600 °C and an α to β structure phase transition occurred between 100 °C and 200 °C.

Acknowledgments

The authors thank the Nation Natural Science Foundation of China (No. 50372027), the Nature Science Foundation for Key Basic Research of Jiangsu Higher Education Institution of China (No. 06KJA43010), Yangzhou Uinversity Development Foundation for Talents (No. 0274640015427) and Yangzhou University Science and Technique Innovation Foundation (No. 2010CXJ081).

References

[1] T.A. Mary, J.S.O. Evans, T. Vogt, Science 272 (1996) 90.
[2] J.S.O. Evans, T.A. Mary, T. Vogt, Chem. Mater. 8 (1996) 2809.
[3] J.E. Readman, S.E. Lister, L. Peters, J. Wright, J.S.O. Evans, J. Am. Chem. Soc. 131 (2009) 17560.
[4] N.A. Banek, H.I. Baiz, A. Latigo, C. Lind, J. Am. Chem. Soc. 132 (2010) 8278.
[5] L.M. Sullivan, C.M. Lukehart, Chem. Mater. 17 (2005) 2136.
[6] K. Haman, P. Badrinarayanan, M.R. Kessler, ACS Appl. Mater. Interfaces 1 (2009) 1190.
[7] J.C. Chen, G.C. Huang, C. Hu, J.P. Weng, Scripta Materialia 49 (2003) 261.
[8] L.F. Zhang, J.Y. Howe, Y. Zhang, H. Fong, Cryst. Growth Des. 9 (2009) 667.
[9] M.S. Sutton, J. Talghader, J. Microelectromech, Syst. 13 (2004) 688.
[10] X.J. Sun, J. Yang, Q.Q. Liu, X.N. Cheng, J. Alloys, Compd. 481 (2009) 668.
[11] S. Nishiiyama, T. Hayashi, T. Hattori, J. Alloys, Compd. 417 (2006) 187.
[12] X.B. Yang, X.N. Cheng, X.H. Yan, J. Yang, Comp. Sci. Technol. 67 (2007) 1167.
[13] P. Lommens, C.D. Meyer, K.D. Bruneel, J. Eur. Ceram. Soc. 25 (2005) 3605.
[14] C. Verdon, D.C. Dunand, Acta. Metall. 39 (1997) 1075.
[15] H. Holzer, D.C. Dunand, J. Mater. Res. 14 (1999) 780.
[16] S. Yimaz, Comp. Sci. Technol. 62 (2002) 1835.
[17] L.D. Noailles, H.H. Peng, J. Starkovich, B. Dunn, Chem. Mater. 16 (2004) 1252.
[18] Z.J. Xiao, X.N. Cheng, X.H. YAN, Sur. Coat. Technol. 201 (2007) 5560.
[19] J.S.O. Evans, Z. Hu, J.D. Jorgensen, D.N. Argyrious, S. Short, A.W. Sleight, Science 275 (1997) 61.
[20] A.W. Sleight, Inorg. Chem. 37 (1998) 2854.
[21] A.K.A. Pryde, K.D. Hammonds, M.T. Dove, V. Heine, J.D. Gale, M.C. Warren, J. Phys, Condens, Matter 8 (1996) 10973.
[22] C. Dong, J. Appl. Cryst. 32 (1999) 1836.